minerals

Article

Origins and Geochemistry of Oolitic Dolomite of the Feixianguan Formation from the Yudongzi Outcrop, Northwest Sichuan Basin, China

Liya Zhang [1,*], Yangquan Jiao [2], Hui Rong [2], Rong Li [3] and Rui Wang [4]

1. Key Laboratory of Submarine Geosciences, Second Institute of Oceanography, State Oceanic Administration, Hangzhou 310012, China
2. Key Laboratory of Tectonics and Petroleum Resources (China University of Geosciences), Ministry of Education, Wuhan 430074, China; yqjiao@cug.edu.cn (Y.J.); ronghui0411@gmail.com (H.R.)
3. Department of Earth and Atmospheric Sciences, University of Alberta, Alberta, AB T6G1H7, Canada; rli4@ualberta.ca
4. School of Marion Sciences, Guangxi University, Nanning 530004, China; wr1983@eyou.com

* Correspondence: liyazhangmail@126.com

Received: 14 June 2017; Accepted: 12 July 2017; Published: 16 July 2017

Abstract: The topic of dolomite formation has long presented a challenge to researchers. In this study, the origin of widely occurring oolitic dolomites from the Yudongzi outcrop in the lower Triassic Feixianguan formation in northwest Sichuan, China, was investigated through petrographic observations, and mineralogical and geochemical analysis. Analytical methods used include cathodoluminescence, X-ray diffraction, stable isotopes, and electronic microprobe characterization. The dolomites were categorized into three major genetic types according to their textural and structural characteristics, which reflect their various origins. The first genetic type of these dolomites, seepage reflux dolomitization, occurs in marly to microcrystalline dolomite during the penecontemporaneous stage, and displays negatively skewed $\delta^{18}O$ (-2.83‰ Pee Dee Belemnite (PDB)), positively skewed $\delta^{13}C$ (2.71‰ PDB), a low degree of order (0.48), and $^{87}Sr/^{86}Sr$ ratios of 0.707509–0.707634, indicating involvement of a Mg-rich brine fluid in an open evaporative environment. The second type, shallow burial dolomitization, is the most significant genetic type of dolomite reservoir in this area. This process produced dominantly silty to fine crystalline dolomite in a platform-margin oolitic beach facies with negatively skewed $\delta^{18}O$ (-3.26‰ PDB), positively skewed $\delta^{13}C$ (1.88‰ PDB), a high degree of order (0.70), and $^{87}Sr/^{86}Sr$ ratios of 0.707318–0.707661, which are related to seawater-derived fluids in a shallow burial environment. The third type is moderate to deep burial dolomitization, and is the main process responsible for zoned dolomite and dolomite with cloudy cores and clear rims (CCCR dolomite), which have the most strongly negatively skewed $\delta^{18}O$ (-7.32‰ PDB), positively skewed $\delta^{13}C$ (3.02‰ PDB), and $^{87}Sr/^{86}Sr$ ratios of 0.707217–0.707855, representing diagenetic alteration and fluid flow in a closed environment. These findings indicate that dolomite was likely affected by various degrees of burial and related marine-derived fluids, which will aid exploration efforts in high-quality hydrocarbon reservoirs in the Sichuan Basin.

Keywords: oolitic dolomite; origins of dolomite; geochemical characteristics; Feixianguan formation

1. Introduction

Dolomite is one of the most important reservoir rock types in the world: around one-third of oil and gas resources occur in carbonate reservoirs, of which half are composed of dolomite [1,2]. Since the first description of dolomite by a French naturalist in 1791 [3], the origin of both the mineral and rock form of dolomite has met with considerable controversy for over two hundred years. As studies on dolomite reservoirs have progressed and expanded, various formation mechanisms and dolomite deposition models have been proposed by sedimentologists, including seepage reflux [4–7], evaporation pumping [8,9], mixed water [10–13], and burial dolomitization [14–17]. These models have been widely used to explain the origin and stratigraphic distribution of ancient platform carbonates. However, for saddle dolomites which are characterized by coarse-crystalline white dolomite aggregates with curved crystal facies, commonly associated with higher temperatures and structures such as broken layers, thrust belts, and tectonized rocks beneath impermeable caprocks, hydrothermal fluids are likely to be involved in the dolomitization process. Current research has increasingly focused on structurally controlled hydrothermal dolomite (HTD) reservoirs [18–21], following on from earlier discoveries in the Ordovician Lima–Indiana field, and other areas of the northeastern United States [22], as well as the Trenton–Black River in Michigan, and the northern Appalachian basins of the northeastern United States and eastern Canada [23]. Additionally, the global research community is vigorously pursuing the use of anaerobic and aerobic microbial culture experiments to explore nucleation and precipitation mechanisms of obtained material, much of which is very high-magnesium calcite, rather than dolomite [24,25]. Several researchers have proposed microbial and organogenic models of this "dolomite" formation, which emphasize the importance of metabolic activity in microbial carbonate precipitation [26–29].

Over the last 30 years, oolitic dolomite reservoirs have come to represent a resource of increased economic value, and have become the subject of extensive research, such as the oolitic dolomites of the Mississippian Ste. Genevieve Group in the North Bridgeport oil fields of the Illinois Basin in the U.S. [30], and the oolitic dolomites in the Puguang gas field in the lower Triassic Feixianguan formation of the Sichuan Basin in China [31,32]. Using mineralogical, petrological, and geochemical methods, many oil and sedimentary scientists have conducted intensive research on the widely occurring dolomite reservoirs in the Sichuan Basin. These workers have proposed a number of dolomitization models, such as seepage reflux and mixed water dolomitization [32–36], burial dolomitization related to burial in a closed marine system [37–40], and tectonically controlled hydrothermal dolomitization characterized by saddle dolomites [41–46]. To a certain extent, these results represent the current state of knowledge of dolomitization mechanisms; however, many problems remain unresolved, such as the source and nature of the mineral-forming fluid, and the time scales and dynamics involved in dolomization and dissolution of the carbonate rock, among others. In the northwestern Sichuan Basin, previous studies have documented the various reservoir properties, diagenetic features, and internal structures of oolitic beach reservoirs in the lower Triassic Feixianguan formation in Erlangmiao, Jiangyou [47–51], however, these works have not thoroughly investigated the origins of the dolomite. This study conducted a detailed petrographic characterization through mineralogical and geochemical analyses using cathodoluminescence (CL), stable isotopes, X-ray diffraction, and electron microprobe methods to investigate the oolitic dolomites from the Yudongzi outcrop in the Feixianguan Formation, in order to constrain the most likely origin of the dolomite, and therefore promote further exploration efforts in high-quality reservoirs.

2. Geological Setting

The Yudongzi outcrop is located at the southern boundary of the Tianjingshan anticline at a distance of about 10 km from northwestern Erlangmiao in the Jiangyou region in the Sichuan Basin. This area is a Late Mesozoic–Cenozoic foreland basin located at the northwest margin of the Yangtze platform between the Longmenshan fold belt, the Dabashan fold belt, and the Yunnan–Guizhou–Hubei fold belt (Figure 1a) [52]. From west to northeast, the distribution of paleogeographical environments of early Feixianguan sedimentary facies is alluvial fan/fluvial facies, marine/terrigenous facies, semi-confined marine facies, carbonate platform facies, and facies associated with the Kaijiang–Liangping Trough and the Chengkou–Western Hubei Trough [53]. The Yudongzi outcrop is located in a carbonate platform margin controlled by the Western Sichuan Trough and the Guangwang–Kaijiang–Liangping Trough (Figure 1b) [51].

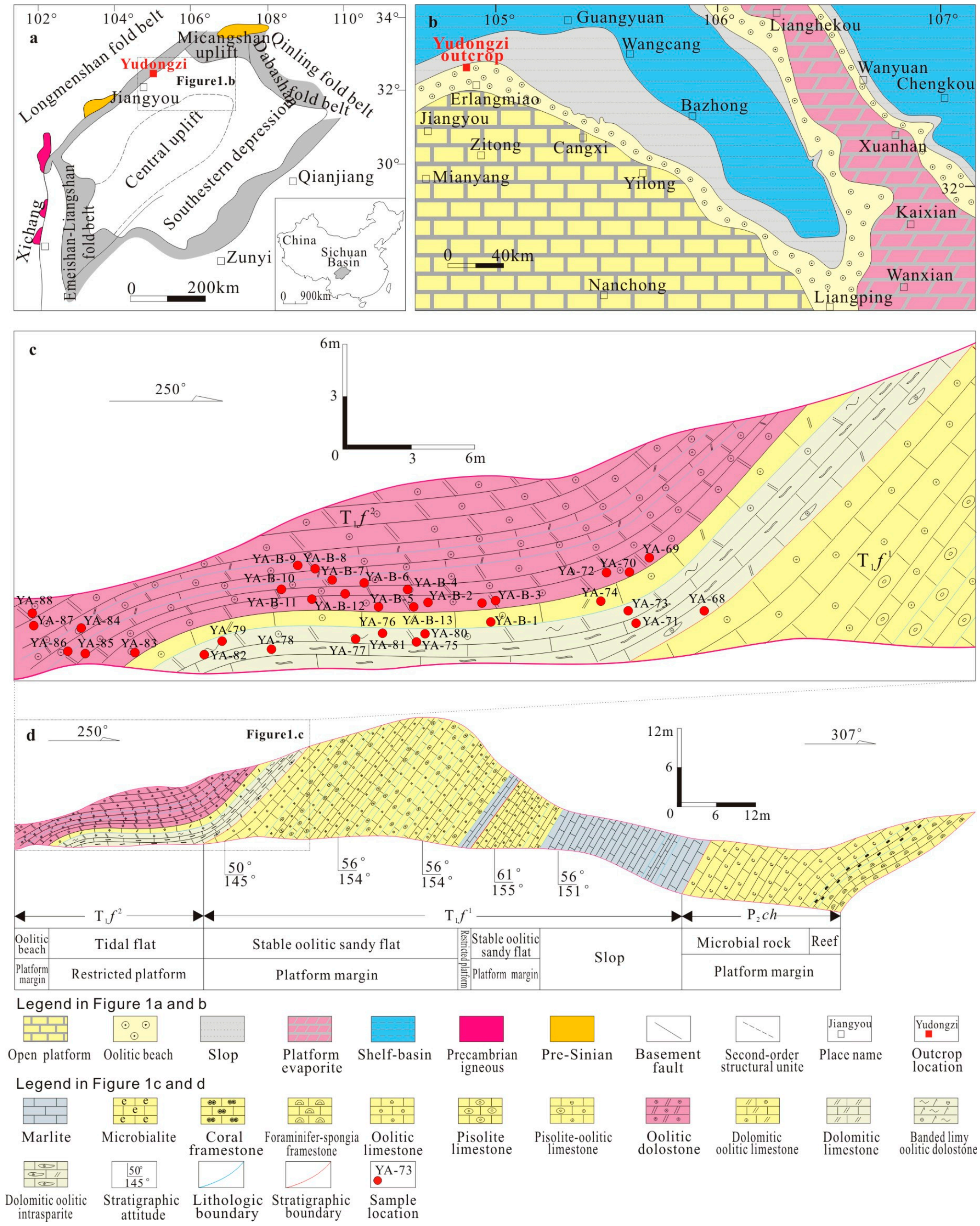

Figure 1. Sedimentary facies and sampling location of the Yudongzi outcrop in the Lower Triassic Feixianguan Formation (modified from Rong, H. et al., 2012 [49]).

The primary strata exposed in this area are the Lower Permian Changxing Formation (P_2ch) and the Lower Triassic Feixianguan Formation (T_1f) (Figure 2a,b), which can be divided into four sections termed T_1f^1, T_1f^2, T_1f^3, and T_1f^4, from bottom to top, respectively. P_2ch is composed of reefs, microbial–bioclastic rocks, and foraminifer–spongia framestones. T_1f^1 and T_1f^2 are characterized by marly limestones, oolitic dolostones, and oolitic grainstones, while T_1f^3 and T_1f^4 are composed of halite rocks, gypsum rocks, and marly microcrystalline limestones and dolostones [51,54,55]. The dolostones from this outcrop investigated here occur dominantly in T_1f^2, and are primarily composed of residual oolitic dolostones, gray dolostones, and dolomitic oolitic grainstones (Figure 2c,d).

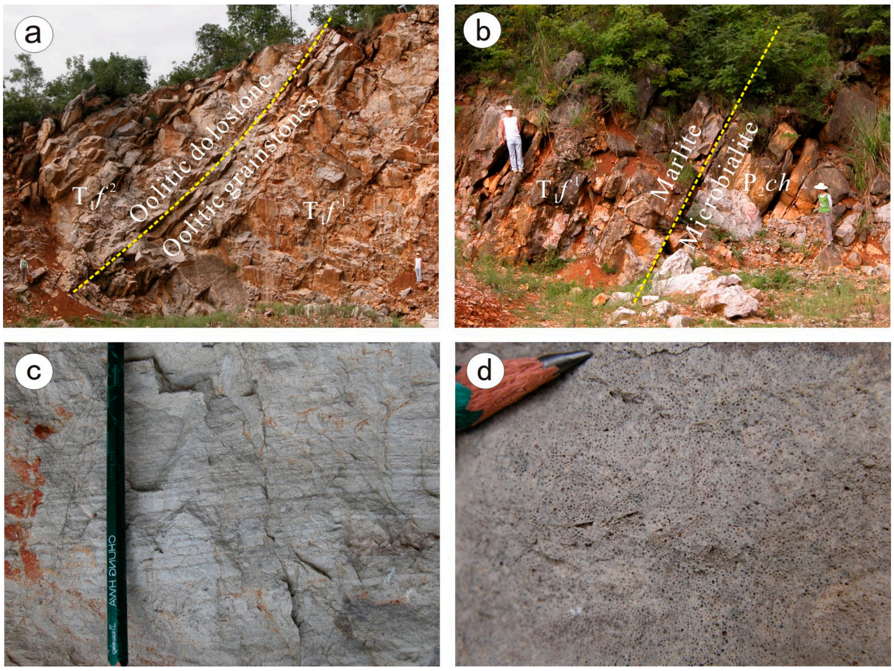

Figure 2. Field and macroscopic features of rocks from the Yudongzi outcrop. (**a**) Boundary between oolitic grainstone of T_1f^1 and oolitic dolostone of T_1f^2. (**b**) Boundary between marlite of T_1f^1 and microbialite of P_2ch. (**c**) Banded gray oolitic dolostones in the bottom of T_1f^2. (**d**) Residual oolitic dolostones in the middle of T_1f^2.

3. Materials and Methods

A total of 34 dolomite samples were analyzed in this study, of which 22 samples represent an active platform-margin oolitic beach environment, and 12 samples represent a tidal flat environment (Figure 1c,d). The strength of dolomitization in T_1f^2 gradually increases from bottom to top vertically, presenting a change in lithology from gray dolomite to residual oolitic dolomite. For this study, mineralogical and geochemical characterization was conducted using CL, X-ray diffraction, stable isotopes, fluid inclusion, and electronic microprobe analysis methods in the State Key Laboratory of Geological Processes and Mineral Resources at the China University of Geosciences (Wuhan).

Petrographic thin sections were prepared including alizarin red and cast thin section analysis, and observed using a Nikon optical microscope to identify dolomite types. Cathodoluminescence was performed using a CL8200-MK5 instrument (Cambridge Image Technology Ltd., Hertfordshire, UK) with a Leica polarizing microscope in the Key Laboratory of Tectonics and Petroleum Resources at a beam voltage of 15 kV and a beam current of 280 μA.

X-ray diffraction (XRD) patterns were collected using an X'pert MPD Pro diffraction analyzer imported from Panalytical analytical instruments Inc., Almelo, The Netherlands, with measurement conditions of 22 °C and 65% humidity. Samples for X-ray diffraction consisted of 5 g of sample material that was crushed to a 200 mesh grain size in an agate mortar. On the basis of the Rydberg Formula and the wavelength values (λ = 0.15418 nm) of Cu target under the working conditions of the diffractometer tube with a voltage of 40 kV and a current of 40 mA, the XRD patterns were qualitatively analyzed by the MDI Jade 6.5 software (USA Materials Data Inc., Livermore, CA, USA). Electron microprobe analysis was conducted on a JEOL JXA-733 instrument imported from the JEOL Ltd. (Tokyo, Japan). The concentrations of oxides of Na, Sr, Mn, Fe, and other elements were analyzed at accelerating voltages in the range 10–25 kV. The total error range of the quantitative analysis is 3%, and external reproducibility of standards is less than 5%.

Samples for carbon and oxygen isotope analysis were prepared by crushing 50 mg of sample material to a grain size of 200 mesh in an agate mortar. These were further processed by flotation and purification in a CCl_4 solution after drying at 100 °C, after which they were placed into a glass cylinder at a temperature of 475 ± 1 °C for 60 min to remove attached organic matter. A Finnigan MAT251 mass spectrometer (Thermo Electron Corporation, Waltham, MA, USA) was used for the measurements, which has a standard error of 0.1‰ of the standard sample GBW04406. Samples were dissolved in a 100% phosphoric acid at a constant temperature of 25 °C for 72 h, collecting the CO_2 gases from the phosphate decomposition at 24 h later to 72 h, with results reported relative to the PDB standard. Strontium isotopes were analyzed on a Triton TI thermoelectric isotope mass spectrometer (Thermo Fisher Scientific Inc., Waltham, MA, USA). Seventy mg of sample material was crushed to a size of 200 mesh, and dissolved in HNO_3 and HF acids, then placed into a solution bottle for about 48 h at 190 °C. The National Bureau Standard NBS987 was used as a standard sample, which has a $^{87}Sr/^{86}Sr$ value of 0.710256 ± 9 (2 δm). The error range is 0.000005–0.000017.

Fluid inclusion measurements were conducted on a Linkam MDS 600 stage (Linkam Scientific Instruments Ltd., Surrey, UK). The precision of the temperature measurements during cooling and heating was approximately ±0.1 °C and ±2 °C, respectively.

4. Results and Discussion

4.1. Mineralogical Characteristics of Dolomite

4.1.1. Genetic Classification

Thin sections from a total of 34 samples were petrologically characterized, and the dolomite was classified as one of the three following types according to the mineralogical composition, texture, and grain size, as well as genetic features.

(1) **Marly to microcrystalline dolomite:** This type occurred in the tidal flat facies at the bottom of T_1f^2. It has relatively low porosity with poor connectivity. At both the outcrop scale and the microscope scale, algae-related mud banding and layered bird-s eye-like structures can be observed (Figure 3a,b), along with evidence of penecontemporaneous intertidal/supratidal exposure. The sedimentary bedding microstructure is well preserved and the dolomite crystals have an anhedral habit. In the oolite interiors, clear geopetal structures and stylolites can be seen (Figure 3a). The dolomite appears dark red in CL images (Figure 4a), indicating that they experienced strongly reducing conditions in a burial environment.

(2) **Silty to fine crystalline dolomite:** This type occurs throughout the periodic exposures of the platform-margin oolitic beach facies in the upper and middle part of T_1f^2. It is primarily composed of oolitic dolomite, which contains rich oolitic molds and intergranular pores. The dolomite grains are subhedral to euhedral crystals, with equal proportions of massive and comb-like textures, representing a second generation of fine dolomite growth on the external rims of the earlier comb-like silty dolomite in the oolitic particles (Figure 3c). The oolite interior, edges, and concentric laminae consistently exhibit partial or complete dissolution that resulted in pore formation, such as oolitic molds, intragranular dissolution pores, and others (Figure 3d,e). In addition, abundant intergranular pores partially filled with small amounts of microcrystalline calcite and oil were present. The silty to fine crystalline dolomite appears orange–red in CL images (Figure 4b).

(3) **Zoned dolomite and dolomite with cloudy cores and clear rims (CCCR):** This type occurs in oolitic and gray dolomites in the platform-margin oolitic beach facies at the bottom of T_1f^2. The zoned dolomite is euhedral, comb-shaped, and appears clean and light, representing a second-generation cement surrounding the surfaces of the first-generation dolomite, which is silty to fine crystalline (Figure 3f). The dolomite grains appear dark red in CL images (Figure 4c). The CCCR dolomite is a euhedral crystal with cloudy centers and clear rims (Figure 3g). Small amounts of organic matter, residual gray material, and clay occur in the cloudy centers. These dolomites are characterized by strong replacement of oolites and gray matter by interstitial material. A single oolite often substitutes for one or several cross-cutting dolomite crystals. Under CL observation, the dirty, cloudy cores of CCCR dolomite grains appear bright orange–red, while the clear rim are dark or non-luminescent (Figure 4d). The clean annulus appears dark orange–red in CL images. Some CCCR dolomite grains are characterized by a bright extra-annulus (Figure 3h).

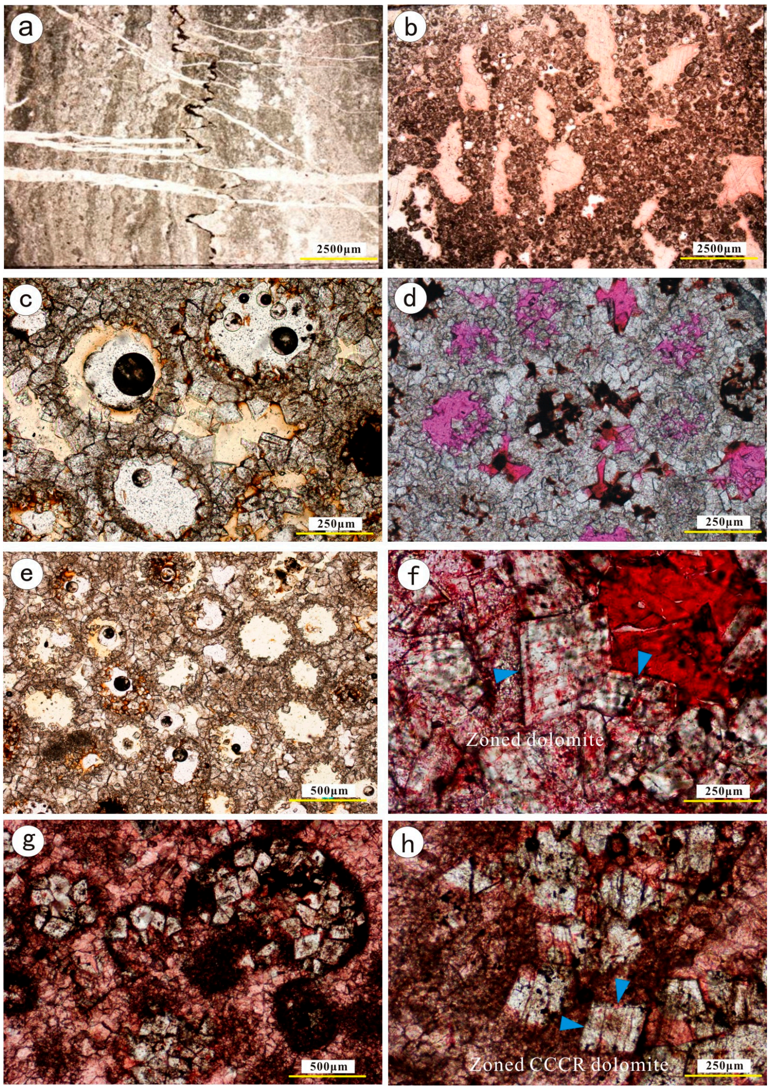

Figure 3. Microscopic features of dolomite from the Yudongzi outcrop. (**a**) Banded marly microcrystalline dolomite from the tidal flat facies with visible layers and stylolites, sample YA-80. (**b**) Marly microcrystalline tidal flat dolomite with dissolution pores filled with calcite, sample YA-77. (**c**) Residual oolitic dolomite from the platform-margin oolitic beach facies showing second-generation fine dolomite overgrowths on the rims of the first-generation comb-like silty dolomite, sample YA-B-12. (**d**) Residual oolitic dolomite from the platform-margin oolitic beach facies with partially filled intragranular and intergranular pores containing oil, sample YA-B-10. (**e**) Residual oolitic dolomite from the platform-margin oolitic beach facies showing comb-like dolomite, sample YA-B-12. (**f**) Residual oolitic dolomite from the platform-margin oolitic beach facies showing zoned dolomite, sample YA-B-2. (**g**) Cloudy cores and clear rims (CCCR) gray dolomite from the platform margin with strong replacement of oolites by one or more dolomite crystals, sample YA-74. (**h**) Zoned CCCR dolomite, sample Ya-74.

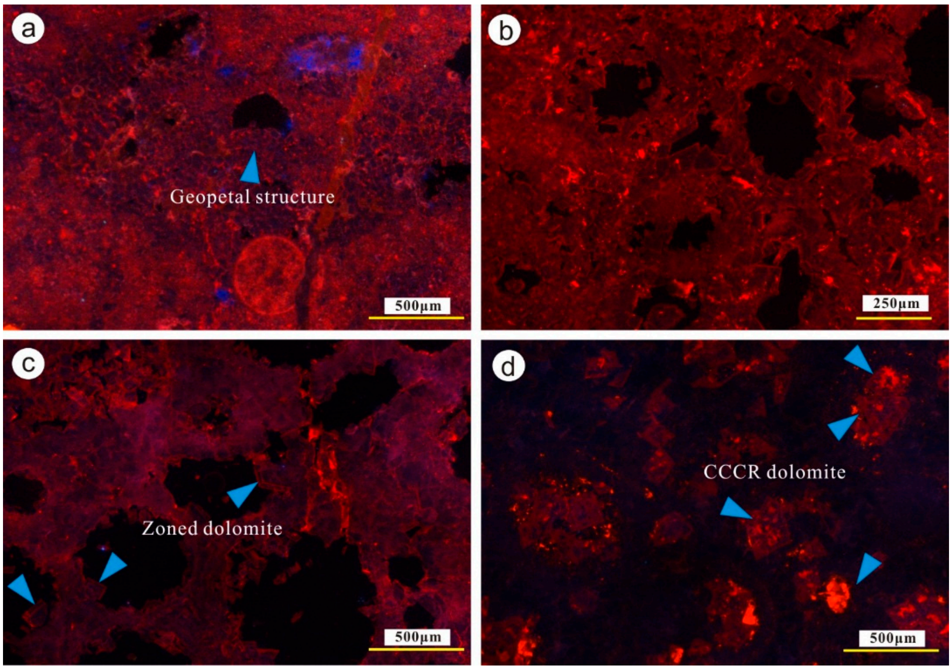

Figure 4. Cathodoluminescence characteristics of dolomite from the Yudongzi outcrop. (**a**) Banded marly microcrystalline tidal flat dolomite with dark red luminescence and geopetal structures, sample YA-80. (**b**) Residual oolitic dolomite from the platform-margin oolitic beach facies with orange-red luminescence, sample YA-84. (**c**) Residual oolitic dolomite from the platform-margin oolitic beach facies with an annulus of dark red luminescence, sample YA-B-12. (**d**) CCCR gray dolomite in the platform-margin oolitic beach facies with cloudy cores in bright orange-red and clear rims with dark or absent luminescence, sample YA-74.

4.1.2. Degree of Order

The degree of order, a significant sign of the crystallinity of dolomite, reflects the arrangement variability of Ca^{2+} and Mg^{2+} ions in dolomite crystal lattices, which of most natural dolomites is between 0 and 1 (the completely ordered dolomite). Commonly, the order degree of dolomite is positively related to the crystallinity, the intensity of dolomitization, and the temperature of nucleation, but negatively related to the molar percentage of $CaCO_3$ [56]. In the process of burial, with the increase of burial depth, the environment temperature is increasing and the Ca^{2+} ions are generally replaced by Mg^{2+} ions, so the degree of order is increasing. Therefore, for the formation of buried dolomite, the deeper the buried depth is, the higher the degree of order is.

Dolomite crystallinity was determined in 26 samples from T_1f^2 located in the platform-margin oolitic beach facies, and 7 samples located in the tidal flat facies, respectively. The results indicate that the degree of order in the silty to fine crystalline oolitic dolomite in the platform-margin oolitic beach facies ranges from 0.55 to 0.92, with an average of 0.70. In these samples, the mole fraction of $CaCO_3$ is greater than 50%, with an average of 53.29% (Table 1). The degree of order in the CCCR or residual gray dolomite in the platform-margin oolitic beach facies ranges from 0.52 to 0.76, with an average of 0.61, and the mole fraction of $CaCO_3$ is greater than 60% with an average of 68.74% (Table 1). The degree of order in the banded or dolomitic oolitic limestone from the tidal flat facies ranges from 0.36 to 0.60, with an average of 0.48, and the mole fraction of $CaCO_3$ is greater than 70%, with an average of 83.17% (Table 1).

Table 1. X-ray diffraction (XRD) data for different dolostone types from the Yudongzi outcrop in the Feixianguan Formation.

Horizon	Rock	Sample	Calcite (mol %)	Dolomite (mol %)	Molar Fraction of Calcium Carbonate (%)	Degree of Order	Genesis
The top of T_1f^2	Gray oolitic dolostone	YA-69	7.84	50.09	56.77	0.84	Shallow burial origin
		YA-70	5.93	51.13	55.2	0.77	
		YA-72	10.55	48.62	58.91	0.79	
		YA-76	7.8	50.11	56.74	0.64	
	Oolitic dolostone	YA-83	0.49	54.08	50.45	0.83	
		YA-84	0	54.35	50	0.9	
		YA-85	4.34	51.99	53.85	0.56	
		YA-86	1.49	53.54	51.35	0.62	
		YA-88	10.28	48.76	58.7	0.63	
		YA-B-2	8.7	49.62	57.46	0.55	
		YA-B-3	6.33	49.03	55.72	0.64	
		YA-B-4	0	54.35	50	0.92	
		YA-B-5	0	54.35	50	0.61	
		YA-B-6	0	54.35	50	0.7	
		YA-B-7	10.38	48.71	58.78	0.59	
		YA-B-8	5.97	51.1	55.23	0.66	
		YA-B-9	0	54.35	50	0.61	
		YA-B-10	0	54.35	50	0.74	
		YA-B-11	0	54.35	50	0.76	
		YA-B-12	0	54.35	50	0.72	
		YA-B-13	0	54.35	50	0.67	
The middle of T_1f^2	Oolitic gray dolostone	YA-73	16.34	45.47	63.22	0.54	Moderate–deep burial origin
	CCCR gray dolostone	YA-74	30.89	33.47	74	0.76	
	Residual oolitic dolostone	YA-77	25.85	40.3	69.54	0.52	
		YA-78	29.41	38.36	71.7	0.69	
	Oolitic gray dolostone	YA-87	19.26	43.88	65.25	0.54	
The bottom of T_1f^2	Residual dolomitic limestone	YA-71	67.64	17.59	89.68	0.45	Seepage reflux origin
	Dolomitic oolitic limestone	YA-75	54.46	24.75	84.38	0.51	
	Banded oolitic limestone	YA-79	52.53	23.6	84.5	0.54	
	Banded oolitic dolostone	YA-80	31.61	37.17	72.98	0.36	
		YA-81	30.06	38.01	72.08	0.42	
	Dolomitic oolitic limestone	YA-82	56.57	23.6	85.28	0.51	
		YA-B-1	77.76	12.09	93.27	0.6	

The degree of order in dolomites from the platform-margin oolitic beach facies is much higher than that in the tidal flat facies (Figure 5). Generally, a high degree of order and a high Mg/Ca ratio reflect slow and complete dolomitization, while a low degree of order indicates fast and incomplete dolomitization [57,58]. The results likely demonstrate that the platform margin experienced prolonged burial at relatively high diagenetic temperatures. Such environments produce relatively low mole fractions of $CaCO_3$ due to the relative lack of competing ions [56]. Accordingly, dolomitization can take place slowly, producing a relatively high degree of order. Conversely, because the tidal flat sediments existed in a high-salinity environment with high rates of sea water evaporation during the Feixianguan period [59,60], the Mg^{2+} content of these rocks is high, which resulted in intense replacement and fast nucleation, ultimately producing marly to microcrystalline dolomites with a low degree of order.

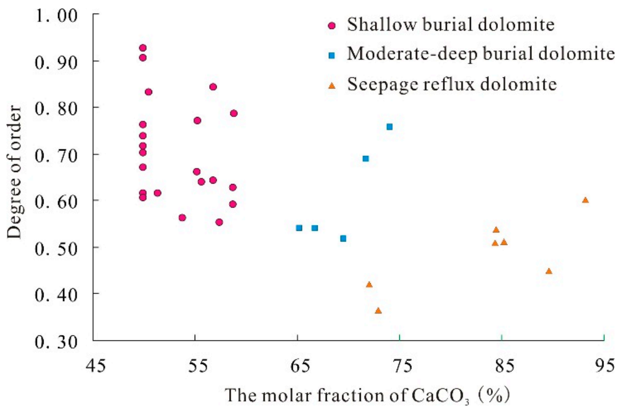

Figure 5. Relation between the degree of order and the molar fraction of calcium carbonate.

4.2. Geochemical Dolomite Characteristics

4.2.1. Iron and Manganese Contents

Most natural dolomite contains minor amounts of iron and manganese, and the variation in the cathodoluminescent properties of carbonates are usually attributed to differing proportions of manganese as the most important activator, and iron as the main inhibitor of luminescence [61]. Besides, the contents of iron and manganese tend to reflect the diagenetic strengths and burial depths. With the increase of buried depths, the rock intensities and Mn and Fe contents increase, and vice versa. This is because under the oxide environment, Mn and Fe are at high-priced states, and have difficulty entering the dolomite lattice [61].

The Fe and Mn contents of dolomites that experienced moderate to deep burial in the platform-margin oolitic beach facies are in the ranges of 1260–1680 mg·kg^{-1} and 50–57 mg·kg^{-1}, respectively, while those of shallowly buried dolomite are in the ranges of 322–980 mg·kg^{-1}and 29–36 mg·kg^{-1}, respectively (Table 2). The former is obviously higher than the latter. In general, the iron and manganese contents of dolomite tend to reflect the intensity of diagenesis and the burial depth, where greater burial depths are associated with stronger diagenesis intensity, and higher Mn and Fe contents [16]. This is because Mn and Fe occur in high-charge states in oxic environments, which inhibits them from entering the dolomite lattice, whereas they occur in low-charge states under the reducing conditions of burial, and can more easily enter the dolomite lattice. Therefore, the Fe and Mn contents indicate that diagenesis in the latter dolomites took place at greater depths than the former type [62].

Table 2. Fe and Mn contents in dolomites from the Yudongzi outcrop.

Horizon	Sedimentary Environment	Rock	Sample	Fe (mg·kg^{-1})	Mn (mg·kg^{-1})	Genesis
The top and middle of T_1f^2	Platform margin oolitic beach	Oolitic dolostone	Ya-84 Ya-86 Ya-B-12	980 322 420	36 26 29	Shallow burial origin
		CCCR gray dolostone	Ya-74	1260	57	Moderate-deep burial origin
		Residual oolitic dolostone	Ya-77	1680	50	
The bottom of T_1f^2	Tidal flat	Banded oolitic dolostone	Ya-80 Ya-81	2170 1820	32 26	Seepage reflux origin

The tidal flat dolomites exhibit the highest Fe contents, ranging from 1820 to 2170 mg·kg^{-1}. This is likely because these sediments were exposed to iron-rich salty seawater, as a result of strong seawater evaporation and poor seawater circulation, under the hot climatic conditions that prevailed during that period [4]. Then, the dolomite lateral infiltration reflows along the platform slope down. These dolomites may also suffer from the post-burial effect.

Electronic microprobe analysis of this type of dolomite revealed that the FeO/MnO ratio of the clear rims is much higher than that in the cloudy cores, resulting in an FeO gradient from low in the cores to high at the edges (Figures 6 and 7). The colors in CL imaging vary from orange-red to dark-red or non-luminescent from the cloudy cores to the clear rims. Typically, CL intensity and colors in dolomite are closely related to the FeO/MnO ratio, where Mn acts as an "activator" and Fe acts as a "quencher" [61]. With increasing FeO/MnO ratios, the luminescence of dolomite gradually changes from bright or light-colored to dark, until it becomes effectively non-luminescent at FeO/MnO ratios of greater than 13 [63]. Therefore, diagenetic fluid alteration can produce annulus in medium to coarse-grained dolomite that reflects the multi-period nature of the fluid during the diagenetic dolomitization process and in the diagenetic burial environment.

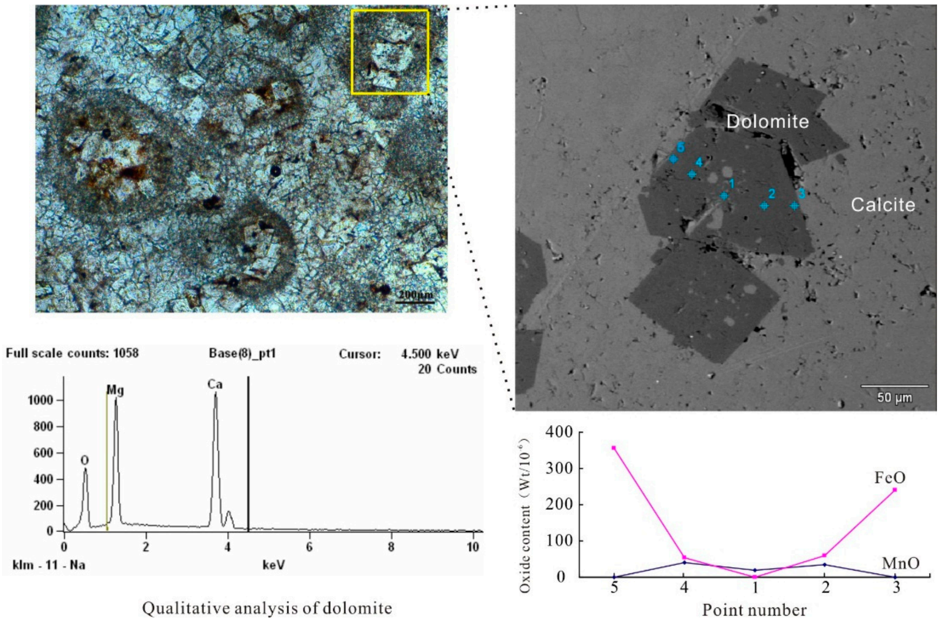

Figure 6. Fe and Mn oxide composition curve of CCCR dolomites (sample YA-74-1).

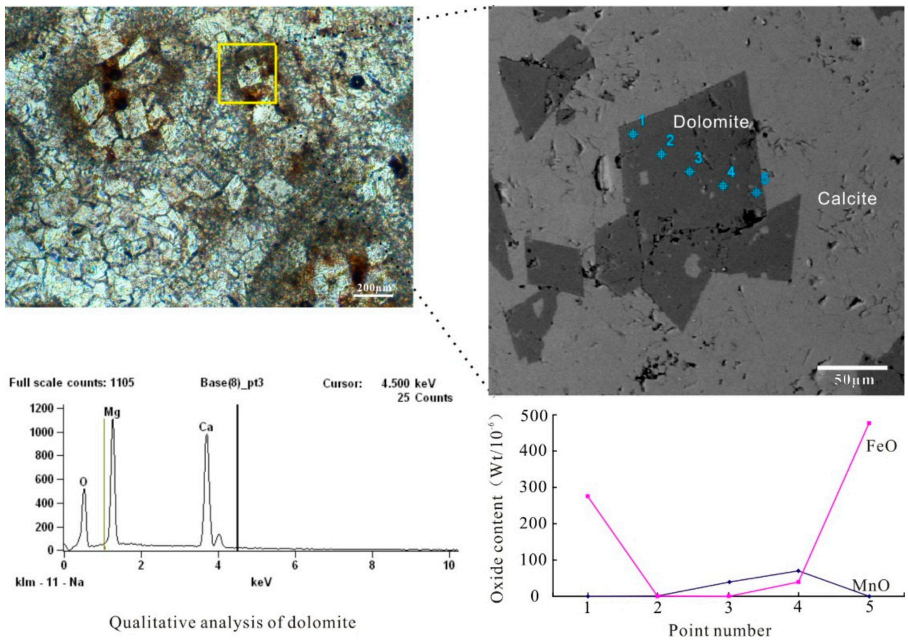

Figure 7. Fe and Mn oxide composition curve of CCCR dolomites (sample YA-74-2).

The cloudy grain centers of CCCR dolomite may have formed at an early stage during burial diagenesis. This is because at depths of several kilometers, especially at temperatures above 60 °C, most natural water tends to convert to a major dolomitizing fluid, such as brines or highly-salinity porewater. In contrast, at low temperatures, dolomite replacement appears to require a long reaction time [64]. However, dolomite formation is inhibited by the quantities of Mg^{2+} supply (mainly through precipitation of residual water and transformation of clay minerals), the influence of temperature and time, the intensity of mass transfer processes and so on [64]. As the nature of the diagenetic fluid changes, dolomite crystals grow rapidly around the nucleus due to rapid replacement of pore water by gray matter [65]. Impurities in carbonate sediments such as clay, organic matter, and gray matter, cannot be expelled from the crystals, and therefore are trapped as inclusions inside the crystal. The clean rims in CCCR dolomite grains likely formed at greater burial depths, as the flow rate slowed.

4.2.2. Carbon and Oxygen Isotopes and Salinity Index

The stable carbon and oxygen isotopic composition in carbonates can reflect different degrees of water–rock interactions. The $\delta^{18}O$ values in dolomite are mainly affected by the temperature, the dilution of meteoric water, evaporation, and so on [66]. For instance, excluding other factors, the increase of temperature and dilution of meteoric water could cause negative skew of $\delta^{18}O$ values, while the decrease of temperature and evaporation could cause positive skew of $\delta^{18}O$ values. ^{13}C in carbonates is mainly derived from the seawater fluids dissolved inorganic carbon or sea-source fluids [67].

Oxygen isotopes were analyzed in 12 dolomite samples from the lower Triassic Feixianguan formation, with values ranging from −7.69‰ to −2.43‰ (PDB). These values are more negative than those of contemporaneous seawater (Table 3), which has $\delta^{18}O$ ranging from −0.8‰ to −0.5‰ (PDB). The $\delta^{13}C$ values vary from +2.8‰ to +3.1‰ (PDB) [68], depending on the various invertebrates and seawater cements present during the different geological periods. The silty to fine oolitic dolomites in the platform-margin oolitic beach facies have negative $\delta^{18}O$ and positive $\delta^{13}C$ values, with average values of $\delta^{18}O$ = −3.26‰ (PDB), $\delta^{13}C$ = 1.88‰(PDB). The oolitic and CCCR gray dolomites in the platform-margin oolitic beach facies have the most negative $\delta^{18}O$ and most positive $\delta^{13}C$ values, with averages of $\delta^{18}O$ = −7.32‰ (PDB), $\delta^{13}C$ = 3.02‰ (PDB). The average $\delta^{18}O$ value of the banded oolitic tidal flat dolomite is −2.83‰, with $\delta^{13}C$ = 2.71‰ (PDB).

Table 3. Carbon and oxygen isotope data for dolomites from the Yudongzi outcrop.

Horizon	Sedimentary Environment	Rock	Sample	$\delta^{13}C$ (‰PDB)	$\delta^{18}O$ (‰PDB)	Z (Salinity Index)	Genesis
The top and middle of T_1f^2	Platform margin oolitic beach	Oolitic dolostone	B-1	1.96	−3.70	129.47	Shallow burial origin
			B-2	1.68	−3.26	129.12	
			B-3	1.95	−2.62	129.99	
			B-4	1.41	−2.52	128.93	
			Ya-84	2.78	−4.73	130.64	
			Ya-86	1.30	−2.43	128.75	
			Ya-B-12	2.11	−3.58	129.84	
		Oolitic gray dolostone	Ya-73	3.59	−6.84	131.25	Moderate-deep burial origin
		CCCR gray dolostone	Ya-74	2.45	−7.44	128.61	
		Residual oolitic dolomite	Ya-77	3.01	−7.69	129.63	
The bottom of T_1f^2	Tidal flat	Banded oolitic dolostone	Ya-80	2.39	−2.52	130.94	Seepage reflux origin
			Ya-81	3.03	−3.13	131.95	

In order to determine the sedimentary environment of carbonate rocks, we take advantage of $\delta^{13}C$ and $\delta^{18}O$ values to calculate Z (salinity index), which is a good indicator of the discrimination between marine facies and continental facies of the carbonate rocks [69], given by the equation: $Z = 2.048 \times (\delta^{13}C + 50) + 0.498 \times (\delta^{18}O + 50)$ (PDB) [69]. Values of $Z > 120$ indicate marine carbonates, while Z < 120, is freshwater carbonate rocks, and when Z = 120, an unfinalized carbonate. All samples in this study yielded Z values greater than 120, indicating that the dolomites are from a marine source.

The tidal flat dolomite has noticeably higher $\delta^{18}O$ values than the platform-margin oolitic beach dolomite (Figure 8), indicating that burial and temperature effects may have influenced the latter dolomite type. These rocks can be further divided into those representing the shallow burial stage, and those from the moderate to deep burial stage, which are distinguished by more negative $\delta^{18}O$ values in the latter compared with the former. Because burial temperatures, water–rock interaction, and atmospheric precipitation affect $\delta^{18}O$ values, increasing temperature causes negatively skewed $\delta^{18}O$ in rocks that would otherwise exhibit positively skewed $\delta^{18}O$ affected by water–rock interaction and atmospheric precipitation (Figure 8) [68]. In high-temperature burial environments, the light isotope ^{16}O preferentially enters the dolomite lattice and the heavy isotope ^{18}O becomes enriched in the diagenetic fluid [70].

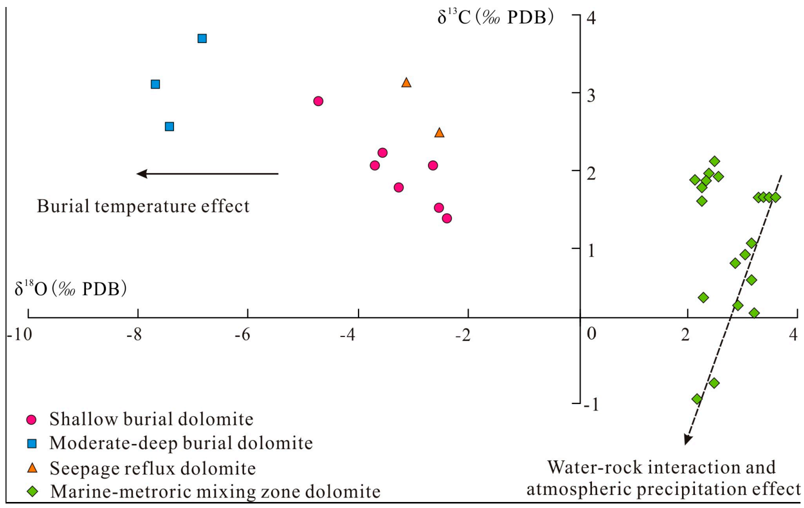

Figure 8. Relation between oxygen and carbon isotopic values in dolomite. The green diamonds data is from Frank and Lohmann (1996) [66].

The different dolomite types have very minor overall variability in $\delta^{13}C$ values (<5%). The carbon isotope values of all dolomite samples range from 1.30‰ to 3.59‰ (PDB) with average values of $\delta^{13}C$ = 2.305‰ (PDB), closed to the corresponding carbon isotopic composition of the Early Triassic global seawater (+2.8‰ to +3.1‰ PDB) [68], indicating the carbon source of these dolomites may inherit the carbon in the calcite (or aragonite) deposited from seawater or marine-source fluid, that is, the carbon source in the dolomitization process is mainly provided by seawater or carbonate dissolution in the same period (near the same period).

4.2.3. Strontium Isotopic Signature and Content

Variations of strontium isotopic ratio and content in the carbonate sediments is most likely the result of the participation of fresh water or brine under the absence of land-based and mantle-derived substances, rather than the isotopic fractionation from physical, chemical, and biological processes [38,40]. In general, in the continent, Sr concentration and $^{87}Sr/^{86}Sr$ ratio in sediments gradually decrease with the increase of fresh water in the porewater, while in the Saabha seabeach, they commonly increase with the rise of the porewater salinity. The Sr isotope composition of the dolomite and non-dolomite is general agreement with that of porewater in the corresponding position.

The strontium isotopic signature and content of eight samples were analyzed and compared (Table 4, Figure 9). Overall, the sample $^{87}Sr/^{86}Sr$ ratios varied between 0.707217 and 0.707855, with an average of 0.707505. From a comparison of the established strontium isotope evolution curve of global marine carbonate rocks, from the early Triassic period with the Feixianguan Formation of northeastern Sichuan, the following conclusions can be reached:

Table 4. Sr contents and isotopic data for dolomites from the Yudongzi outcrop.

Rock	Number	$^{87}Sr/^{86}Sr$		Sr (%)	
		Variation	Average	Variation	Average
Seepage reflux dolomite	2	0.707509–0.707634	0.707572	0.019–0.025	0.022
Shallow burial dolomite	4	0.707318–0.707661	0.707456	0.008–0.016	0.013
Moderate-deep burial Dolomite	2	0.707217–0.707855	0.707536	0.012–0.016	0.014
Marine micrite of Feixianguan Formation [38]	9	0.707330–0.707507	0.707399	0.047–0.310	0.180
Buried dolomite of Feixianguan Formation [38]	37	0.707406–0.708276	0.707659	0.009–0.124	0.021
Global early Triassic marine carbonate rocks [71]	-	0.707650–0.707810	0.707743	-	-

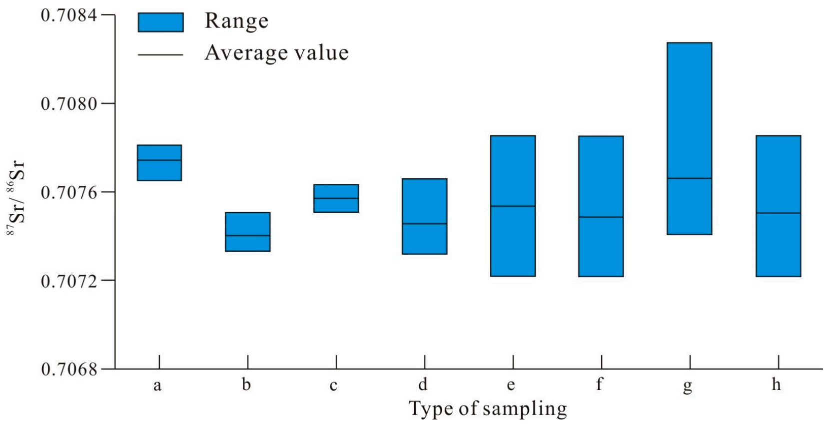

Figure 9. Strontium isotope features of various carbonate rocks of the Feixianguan Formation: (a) Global early triassic marine carbonates [71]; (b) Marine microcrystalline limestone from the Feixianguan Formation [38]; (c) Seepage reflux dolomites from this study; (d) Shallow burial dolomites from this study; (e) Middle-to-deep burial dolomite from this study; (f) All burial dolomite from this study; (g) Group of burial Feixianguan dolomites [38]; (h) All the dolomite samples from this study.

(1) The $^{87}Sr/^{86}Sr$ ratio of marly microcrystalline dolomite from the tidal flat facies ranges from 0.707509 to 0.707634, with an average of 0.707572, which is significantly higher than that of marine micrites from the Feixianguan formation (0.707399) [38]. Generally, increase in the $^{87}Sr/^{86}Sr$ ratio of carbonate sediments results from the influence of brine in the absence of terrigenous substances or mantle-derived material [40]. Thus, the dolomitized fluid is inferred to be related to high-salinity pore water in sediments that were filled with seepage reflux fluid, rather than seawater in an exposed environment.

(2) The $^{87}Sr/^{86}Sr$ ratio of shallow burial dolomite from the platform-margin oolitic beach ranges from 0.707318 to 0.707661, with an average of 0.707456, the lower limit of which is close to that of Feixianguan seawater (0.707399) [38], and the upper limit is close to that of seepage reflux dolomite in this study (0.707634). This indicates that the dolomitizing fluid underwent substantial interaction with the Feixianguan seawater and the infiltration–refluxing fluid, generating the properties of a marine fluid.

(3) The $^{87}Sr/^{86}Sr$ ratio of dolomite from the mid-to-late burial stage ranges from 0.707217 to 0.707855, with an average of 0.707536. This average value is close to that of Feixianguan burial dolomites in the northeastern Sichuan Basin (0.707659) [38], and the upper limit is close to that of global marine early Triassic carbonates (0.707810) [71]. This finding is consistent with the possibility

that the fluid responsible for the formation of this dolomite is related to a marine-derived burial dolomitization fluid in a closed environment, in which Mg^{2+} originated from pore water, interlayer water produced by clay mineral transformation and so on.

The range of Sr contents in various carbonate rocks of the Feixianguan formation is shown in Table 4. The Sr content of marly microcrystalline dolomite from the tidal flat facies ranges from 0.019% to 0.025% with an average value of 0.022% (Table 4). This value is close to the value of 0.025% of ultra-saline seawater formed during penecontemporaneous dolomite precipitation [72], indicating that the Feixianguan seawater has a high strontium content in this area, which is associated with global aragonite-based strontium-rich deposition in the early Triassic.

The Sr contents of shallow burial dolomites from the platform-margin oolitic beach facies lie in the range of 0.008–0.016%, with an average value of 0.013%, while those of moderate to deep burial dolomite range from 0.012% to 0.016%, with an average of 0.014%. Both rock types from different burial stages have significantly higher Sr contents than that of a HTD from an alpine basin in Canada, which has a range of 0.0037–0.0122% [73].

The dolomitization process is ultimately one of Sr loss [38]. In Sr-rich carbonates from the Early Triassic Feixianguan period and in early Carboniferous sediments, strontium removal may occur at the onset of aragonite dissolution and recrystallization in the absence of continental freshwater [38,74]. This could explain why the Sr content decreases from 0.22% to 0.13–0.14% from the surface to greater depths, indicating an increase in dolomitization intensity. The similar Sr contents in both types of burial dolomite likely indicate that the dolomitization process occurred in a relatively closed system.

4.3. Fluid Inclusions

Small amounts of gas–liquid or bitumen inclusions in grains of CCCR dolomite were identified in this study, however, inclusions in marly to silty dolomite are too small to identify. The homogenization temperatures determined in five samples range from 172.3 °C to 241.4 °C, with an average salinity of 10.5% (NaCl wt % eqv). Most of the fluid inclusions have salinities higher than that of normal seawater (3.5%).

We employed the experimental oxygen isotope calibration of dolomite from Horita (2014) [75] to calculate the values of $\delta^{18}O_{water}$, in which the dolomite–water equilibrium fractionation factor for a wide range of the temperature interval between 80 °C and 350 °C (176 °F and 662 °F). The oxygen isotopic composition of the dolomitizing fluid can be reversed by the oxygen isotope fractionation equation as follows [75]:

$$10^3 \ln \alpha_{\text{dolomite–water}} = 3.140\ (\pm 0.022) \times \frac{10^6}{T^2} - 3.14\ (\pm 0.11) \tag{1}$$

$$\alpha_{\text{dolomite–water}} = \frac{(^{18}O/^{16}O)_{\text{dolomite}}}{(^{18}O/^{16}O)_{\text{water}}} = \frac{\delta^{18}O_{\text{dolomite}} + 10^3}{\delta^{18}O_{\text{water}} + 10^3} \tag{2}$$

Taking the logarithm on both sides of Equation (2), we can draw the equation:

$$10^3 \ln\alpha_{\text{dolomite-water}} = \delta^{18}O_{\text{dolomite}} - \delta^{18}O_{\text{water}} \tag{3}$$

Here, $\alpha_{\text{dolomite–water}}$ is the oxygen isotope fractionation coefficient between dolomite and water, T is the absolute temperature in units of Kelvin, and the $\delta^{18}O$ standard is standard mean ocean water (SMOW, ‰). Then, the $\delta^{18}O_{PDB}$ of the carbonates could be converted to $\delta^{18}O_{SMOW}$ values, using the same conversion formula for SMOW and PDB [76]: $\delta^{18}O_{SMOW} = 1.03091\delta^{18}O_{PDB} + 30.91$. The above Equations (1) and (3) could be used to reverse the oxygen isotope composition ($\delta^{18}O_{\text{dolomitization fluid}}$), on the basis of the oxygen isotopic composition of dolomite minerals ($\delta^{18}O_{\text{dolomite}}$) and the precipitation temperature (T) corresponding to the homogenization temperatures of inclusions of dolomites.

Previous studies have demonstrated that the $\delta^{18}O$ values and homogenization temperatures of inclusions of marly to microcrystalline dolomite samples from the lower Triassic Feixianguan formation range from −4.31 to −7.24‰PDB, and 40 °C to 42 °C, respectively [77]. According to the $\delta^{18}O_{dolomite}$ values and the homogenization temperatures of inclusions in the CCCR dolomite from the platform-margin oolitic beach, the calculated $\delta^{18}O_{dolomitization\ fluid}$ values fall between +10‰ and +15‰ (SMOW) (Figure 10), around the seawater line far from the atmospheric waterline. It can be concluded that the dolomitizing fluid was likely a high-salinity, high-temperature burial fluid, indicating that moderate to deep burial dolomitization produced this type of dolomite. The calculated $\delta^{18}O_{dolomitization\ fluid}$ values of marly microcrystalline dolomite from Mu et al. (1994) [77] range from −6‰ to −2‰ (SMOW) (Figure 10), which are close to that of high-magnesium contemporaneous seawater, and likely reflect a strong influx of meteoric waters that shifted the oxygen isotopes to more negative values, assuming a value for global open marine Triassic seawater of $\delta^{18}O$ = 0‰ (SMOW) [78], which is the continuous stable isotope baseline trends from a dataset of δ^{13} C and $\delta^{18}O$ values of well-preserved Triassic brachiopods and carbonate rocks. Calculating a water value from homogenization temperature and dolomite $\delta^{18}O$ should ensure all samples are under the same conditions; considering the complicated diagenetic history of these samples, this result is likely not precisely true.

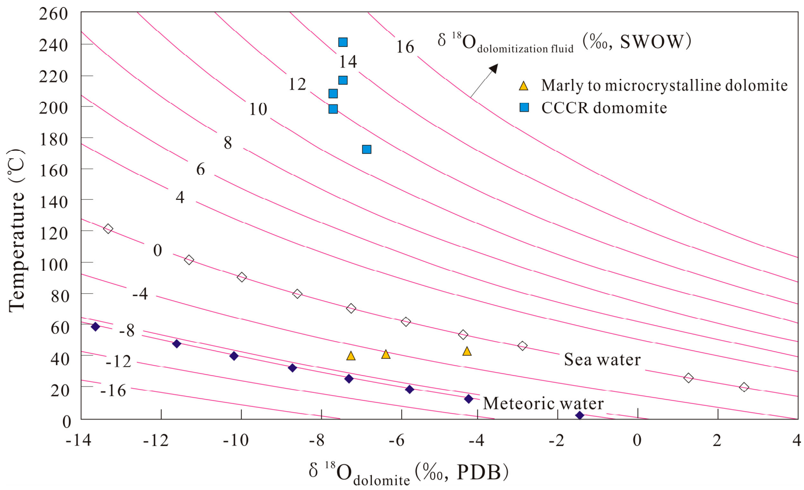

Figure 10. Relation between the oxygen isotope composition and inclusion homogenization temperatures in dolomite (the errors are smaller than the symbols). Contours represent the oxygen isotope composition of dolomitization fluid, calculated by the formula from Horita (2014) [75]. The contour line with hollow diamond points is the $\delta^{18}O$ curve for global Triassic seawater, assuming a global Triassic seawater value of 0‰ (standard mean ocean water (SMOW)) [78]; The contour line with solid diamond points is the $\delta^{18}O$ curve of meteoric water with an average of −8.35‰ (SMOW) [79].

4.4. Origins of Dolomite

4.4.1. Seepage Reflux Dolomitization

The origin of the marly to microcrystalline dolomite can be suitably explained by a seepage reflux dolomitization mechanism that occurred primarily during the syndiagenetic/penecontemporaneous stage, when climatic conditions in the tidal flat changed from warm and humid, to dry and hot. The Mg-rich brine formed in this evaporative environment likely flowed along the platform-margin oolitic beach, where it laterally penetrated the sediments and flowed back after mixing with the pore water [59]. This dolomite replaced deposits of aragonite mud and micrite, forming marly microcrystalline dolomite with geochemical features characterized by relatively negatively skewed

$\delta^{18}O$, positively skewed $\delta^{13}C$, a low degree of order, and a high $^{87}Sr/^{86}Sr$ ratio, influenced by post-burial effects.

4.4.2. Shallow Burial Dolomitization

Shallow burial dolomitization occurred mainly in the platform-margin oolitic beach environment to produce silty to fine-grained dolomite. Under these shallow burial conditions, various fluids including seawater, groundwater, and pore water were able to flow along the seepage channel to the near-surface oolitic reservoir, which provided an abundant source of material for shallow burial dolomitization [80]. Silty to fine-grained dolomite is the most important component of the abundant oolitic dolomite, which contains features such as high concentrations of dissolution pores, cracks, and holes that constitute the best dolomite reservoir properties in this area. Typical genetic markers of this dolomite type have relatively negative $\delta^{18}O$ and positive $\delta^{13}C$ values associated with marine-source fluid, a high degree of order, and high Fe, Mn, and Sr contents.

4.4.3. Moderate to Deep Burial Dolomitization

Increasing burial depth and diagenetic intensity favor intense dolomite formation. Under high-temperature and reducing conditions in a closed environment, dolomite crystals were rapidly replaced to form zoned and CCCR dolomite. However, as the Mg^{2+} supply was highly limited during moderate-deep burial, Mg^{2+} was derived mainly from the transformation of pore water and clay minerals. This may explain why the dolomite distribution is dispersed throughout the oolitic gray dolostones. The typical genetic markers of this dolomite are relatively negative $\delta^{18}O$ values, high Fe and Mn contents, and a high degree of order, as well as inclusion temperatures of greater than 50 °C. The $^{87}Sr/^{86}Sr$ ratio indicates a marine fluid source in a closed environment.

4.4.4. Proposed Dolomitization Model

A proposed model of dolomite evolution is outlined below and illustrated in Figure 11. The lower Triassic Feixianguan formation is controlled by the Kaijiang–Liangping trough, and the Yudongzi region is located entirely in the platform margin that marks a zone of transition from a carbonate platform to open sea [59]. With the gradual closure of the trough, seawater receded toward the open sea, accompanied by movement of the platform-margin oolitic beaches toward the trough, resulting in the horizontal expansion of these horizons as the climatic conditions changed from warm and humid, to dry and hot [60]. Incomplete exposure of the surface produced strong evaporation of seawater to form a salty Mg-rich fluid in the early period of T_1f^2, while the original tidal flat sediments retained large amounts of pore water. This resulted in downward infiltration of the dolomitizing Mg-rich fluid that flowed in the direction of lower pressure, moving both laterally and vertically, and replacing the limestone to form marly to microcrystalline dolomite through seepage reflux dolomitization.

Continued accumulation of overlying sediments gradually buried the original platform-margin oolitic beach sediments in the mid-late period of T_1f^2. Differences in consolidation and compressive strength between the original sediments and the overlying sediments generated horizontal pressure gradients even at uniform depths, which drove natural water bodies to become dolomitizing fluids at depths of several kilometers [64]. In the shallow burial period, abundant residual oolitic dolomite was formed by dolomitization and dissolution that produced petrological characteristics such as corrosion holes and first-generation comb-like dolomite cements. Ultimately, the dolomitization dynamics decreased significantly under the influence of geothermal gradients and increasing pore fluid temperatures [81], forming zoned and CCCR dolomite crystals with higher crystallinity in a closed burial system.

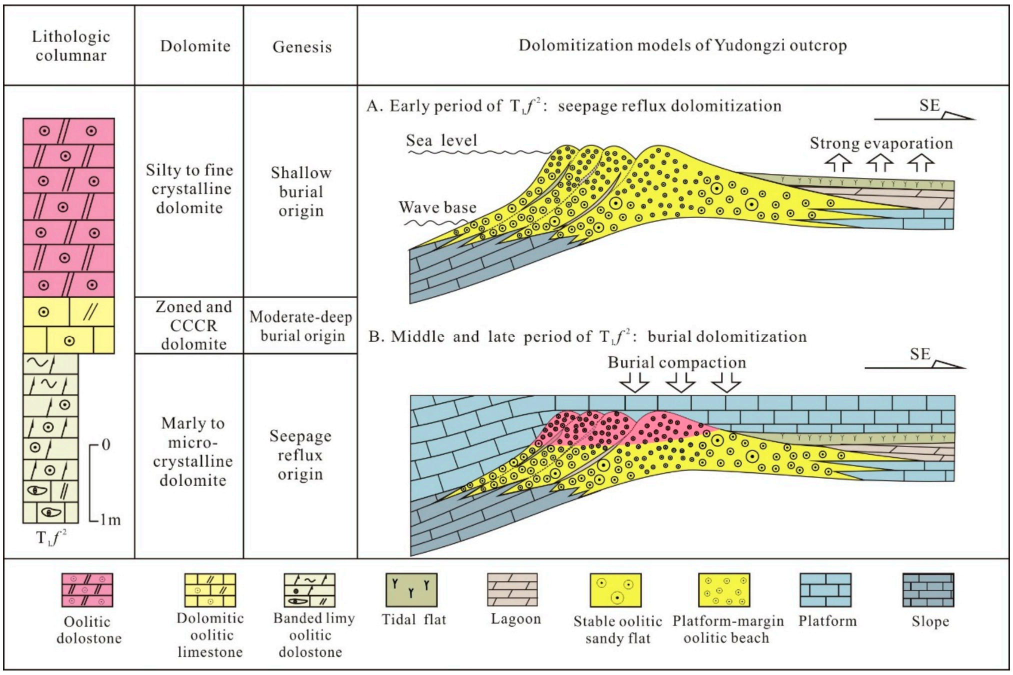

Figure 11. Dolomitization models for rocks of the Yudongzi outcrop.

5. Conclusions

(1) Marly to microcrystalline dolomite from the tidal flat facies is characterized by petrographic features such as algae-related mud-banded sand, and geochemical features such as negatively skewed $\delta^{18}O$ and $\delta^{13}C$ values, a low degree of order, and a high $^{87}Sr/^{86}Sr$ ratio. These properties indicate formation by seepage reflux dolomitization in the penecontemporaneous stage. Post-burial effects may have influenced this type of dolomite.

(2) Silty to fine dolomite from the platform-margin oolitic beach facies is the most significant type of reservoir rock in this region, having been formed by shallow burial dolomitization. These rocks are characterized by high porosity and permeability, with geochemical features marked by negatively skewed $\delta^{18}O$, positively skewed $\delta^{13}C$, high Fe and Mn contents, and a high degree of order. The $^{87}Sr/^{86}Sr$ ratio and Sr contents exhibit properties of marine fluids.

(3) Zoned and CCCR dolomites from the platform-margin oolitic beach facies formed by moderate to deep burial dolomitization, are characterized by strong replacement. FeO/MnO ratios are higher in the clear rims than in the cloudy cores of CCCR dolomite grains. The average inclusion temperature is >50 °C. The dolomitized fluid was shown to have properties consistent with a high-temperature, high-salinity, high-Sr source, which occurred in a relatively closed system. Further modification of this dolomite led to the formation of zoned annules.

Acknowledgments: This research was supported by the Foresight Project of Sinopec Group (YPH08114), the open fund of Key Laboratory of Tectonics and Petroleum Resources (China University of Geosciences), Ministry of Education (TPR-2010-05), and the Central Public-interest Scientific Institution Basal Research Fund (JG1606). Appreciation to the colleagues of Key Laboratory of Tectonics and Petroleum Resources, China University of Geosciences (Wuhan). We are also grateful for the anonymous reviewer's constructive comments and suggestions.

Author Contributions: Yangquan Jiao applied for funding for this work. Liya Zhang conceived, designed, and performed the experiments, analyzed the data, and wrote the original draft; Hui Rong, Rong Li, and Rui Wang collected the samples in the field. Rong Li and Hui Rong discussed the key points with the origins of oolitic dolomite and drew parts of the figures. All the authors reviewed this paper.

Conflicts of Interest: The authors declare no conflict of interest.

References

1. Zenger, D.H.; Dunham, J.B.; Ethington, R.L. Concepts and models of dolomitization: Based on a symposium sponsored by the Society of Economic Paleontologists and Mineralogists. *Tulsa: Soc.* **1980**, *28*, 197–198.
2. Sun, S. Dolomite reservoirs: Porosity evolution and reservoir characteristics. *AAPG Bull.* **1995**, *79*, 186–204.
3. Jan, B.L. Déodat de Gratet de Dolomieu (1750–1801), vie et œuvre d'un géologue européen, naturaliste et lithologiste. *Comptes Rendus De Lacademie Des Sci.* **2000**, *330*, 83–95.
4. Rhodes, J. Dolomitization by seepage refluxion. *AAPG Bull.* **1960**, *44*, 1912–1920.
5. Warren, J. *Evaporites: Their Evolution and Economics*; Blackwell Science: Oxford, UK, 1999; p. 438.
6. Leslie, A.M.; Peter, A.S. Dolomitization of the Capitan Formation forereef facies (Permian, west Texas and New Mexico): Seepage reflux revisited. *Sedimentology* **2002**, *49*, 1207–1227.
7. Fadi, H.N.; Swennen, R.; Ellam, R. Reflux stratabound dolostone and hydrothermal volcanism-associated dolostone: A two-stage dolomitization model (Jurassic, Lebanon). *Sedimentology* **2004**, *51*, 339–360.
8. Friedman, G.M.; Sanders, J.E. Chapter 6: Origin and occurrence of dolostones. *Elsevier Sci. Technol.* **1967**, *9*, 267–348.
9. Hsü, K.J.; Schneider, J. *Progress Report on Dolomitization—Hydrology of Abu Dhabi Sabkhas, Arabian Gulf*; Springer: Berlin/Heidelberg, Germany, 1973; pp. 409–422.
10. Badiozamani, K. The Dorag dolomitization model—Application to the middle Ordovician of Wisconsin. *J. Sediment. Pet.* **1973**, *43*, 965–984.
11. Fookes, E. Development and eustatic control of an Upper Jurassic reef complex (Saint Germain-de-Joux, Eastern France). *Facies* **1995**, *33*, 129–149. [CrossRef]
12. Choquette, P.W.; Steinen, R.P. Mississippian non-supratidal dolomite, Ste. Genevieve Limestone, Illinois Basin: Evidence for mixed-water dolomitizatio. *Spec. Publ.* **1980**, *28*, 163–196.
13. Compton, J.; Harris, C.; Thompson, S. Pleistocene Dolomite from the namibian shelf: High 87Sr/86Sr and 18O values indicate an evaporative, mixed-water origin. *J. Sediment. Res.* **2001**, *71*, 800–808. [CrossRef]
14. Kupecz, J.A.; Kerans, C.; Land, L.S.; Lee, Y.I.; Friedman, G.M. Deep-burial dolomitization in the Ordovician Ellenburger Group carbonates, West Texas and southern New Mexico: Discussion and reply. *J. Sediment. Res.* **1988**, *58*, 908–913. [CrossRef]
15. Mattes, B.W.; Mountjoy, E.W. Burial dolomitization of the Upper Devonian Miette Buildup, Jasper National Park, Alberta. *Polym. Int.* **1980**, *28*, 259–297.
16. Reinhold, C. Multiple episodes of dolomitization and dolomite recrystallization during shallow burial in Upper Jurassic shelf carbonates: Eastern Swabian Alb, southern Germany. *Sediment. Geol.* **1998**, *121*, 71–95. [CrossRef]
17. Wang, G.Z.; Liu, S.G.; Na, L.I.; Dong, W.; Yuan, G. Formation and preservation mechanism of high quality reservoir in deep burial dolomite in the Dengying Formation on the northern margin of the Sichuan basin. *Acta Petrol. Sin.* **2014**, *30*, 667–678.
18. Luczaj, J.A.; Iii, W.B.H.; Williams, N.S. Fractured hydrothermal dolomite reservoirs in the devonian dundee formation of the Central Michigan Basin. *AAPG Bull.* **2006**, *90*, 1787–1801. [CrossRef]
19. Machel, H.G.; Lonnee, J. Hydrothermal dolomite—A product of poor definition and imagination. *Sediment. Geol.* **2002**, *152*, 163–171. [CrossRef]
20. Lavoie, D.; Chi, G. Hydrothermal dolomitization in the Lower Silurian La Vieille Formation in northern New Brunswick: Geological context and significance for hydrocarbon exploration. *Bull. Can. Pet. Geol.* **2006**, *54*, 380–395. [CrossRef]
21. Jiao, C.L.; Zhiliang, H.E.; Xing, X.J.; Qing, H.R. Tectonic hydrothermal dolomite and its significance of reservoirs in Tarim basin. *Acta Pet. Sin.* **2011**, *27*, 277–284.
22. Hurley, N.F.; Budros, R. Albion-Scipio and stoney point fields—USA, Michigan Basin. *AAPG Bull.* **1990**, *23*, 1–37.
23. Smith, L. Origin and reservoir characteristics of Upper Ordovician Trenton—Black River hydrothermal dolomite reservoirs in New York. *AAPG Bull.* **2006**, *90*, 1691–1718. [CrossRef]
24. Gregg, J.M.; Bish, D.L.; Kaczmarek, S.E.; Machel, H.G. Mineralogy, nucleation and growth of dolomite in the laboratory and sedimentary environment: A review. *Sedimentology* **2015**, *62*, 1749–1769. [CrossRef]
25. Kaczmarek, S.E.; Gregg, J.M.; Machel, H.G.; Fouke, B.W.; Bish, D.L. Dolomite, very high-magnesium calcite, and microbes—Implications for the microbial model of dolomitization. *Soc. Sediment. Geol.* **2017**, *109*, 1–14.

26. Korte, C.; Jasper, T.; Kozur, H.W.; Veizer, J. δ 18 O and δ 13 C of Permian brachiopods: A record of seawater evolution and continental glaciation. *Palaeogeogr. Palaeoclimatol. Palaeoecol.* **2005**, *224*, 333–351. [CrossRef]
27. Roberts, J.A.; Bennett, P.C.; González, L.A.; Macpherson, G.L.; Milliken, K.L. Microbial precipitation of dolomite in methanogenic groundwater. *Geology* **2004**, *34*, 277–280. [CrossRef]
28. Kenward, P.A.; Goldstein, R.H.; González, L.A.; Roberts, J.A. Precipitation of low-temperature dolomite from an anaerobic microbial consortium: The role of methanogenic Archaea. *Geobiology* **2009**, *7*, 556–565. [CrossRef] [PubMed]
29. Vasconcelos, C.; Oliveira, C.D. Modern Dolomite Precipitation and Diagenesis in a Coastal Mixed Water System, (Lagoa Vermelha, Brazil): A Microbial Model for Dolomite Formation under Anoxic Conditions. Ph.D. Thesis, ETH Zürich, Zürich, Switzerland, 1994; p. 117.
30. Choquette, P.W.; Steinen, R.P. *Mississippian Oolite and Non-Supratidal Dolomite Reservoirs in the Ste. Genevieve Formation, North Bridgeport Field, Illinois Basin*; Springer: New York, NY, USA, 1985; pp. 207–225.
31. Zhang, X.G.; Rao, D.; Cai, L.G. Pore origin of oolitic dolomite reservoir in Puguang Gasfield. *Nat. Gas Technol.* **2009**, *3*, 11–13.
32. Chen, P.Y.; Tan, X.C.; Liu, H.; Ma, T.; Jiang, X.F.; Yu, Y. Formation mechanism of reservoir oolitic dolomite in Lower Triassic Feixianguan formation, northeastern Sichuan Basin, southwest China. *J. Cent. South Univ.* **2014**, *21*, 3263–3274. [CrossRef]
33. Jiang, L.; Cai, C.F.; Worden, R.H.; Li, K.K.; Xiang, L. Reflux dolomitization of the Upper Permian Changxing Formation and the Lower Triassic Feixianguan Formation, NE Sichuan Basin, China. *Geofluids* **2013**, *13*, 232–245. [CrossRef]
34. Liu, S.G.; Huang, W.M.; Zhang, C.J.; Zhao, X.F.; Dai, S.L.; Zhang, Z.J.; Qin, C. Research status of dolomite genesis and its problems in Sichuan Basin. *Lithol. Reserv.* **2008**, *20*, 6–15.
35. Yang, W.; Hu, M.Y.; Qian, Y. Analysis of dolomitization in Feixianguan Formation in northern Sichuan Basin. *J. Daqing Norm. Univ.* **2011**, *31*, 78–81.
36. Luo, P.; Su, L.; Luo, Z. Application of laser micro-sampling technique to analysis of C and O isotopes of oolitic dolomites in Feixianguan Formation, northeast Sichuan. *Geochimica* **2006**, *35*, 325–330.
37. Huang, S.J.; Qing, H.R.; Hu, Z.W.; Zou, M.L.; Feng, W.L.; Wang, C.M.; Gao, X.Y.; Wang, Q.D. Closed-system dolomitization and the significance for petroleum and economic geology: An example from Feixianguan carbonates, Triassic, NE Sichuan basin of China. *Acta Pet. Sin.* **2007**, *23*, 2955–2962.
38. Huang, S.J.; Qing, H.R.; Pei, C.R.; Hu, Z.W.; Wu, S.J.; Sun, Z.L. Strontium concentration, isotope composition and dolomitization fluids in the Feixianguan Formation of Triassic, Eastern Sichuan of China. *Acta Pet. Sin.* **2006**, *22*, 2123–2132.
39. Huang, S.J.; Qing, H.R.; Hu, Z.W.; Wang, C.M.; Gao, X.Y.; Zou, M.L.; Wang, Q.D. The Diagenesis and dolomitization of the Feixianguan carbonates of triassic in NE Sichuan Basin: An overview. *Adv. Earth Sci.* **2007**, *22*, 495–503.
40. Zheng, R.C.; Wen, H.G.; Zheng, C.; Luo, P.; Li, G.J.; Chen, S.C. Genesis of dolostone of the Febdanguan Formation, Lower Triassic in the NE Sichuan basin: Evidences from rock structure and strontium content and isotopic composition. *Acta Pet. Sin.* **2009**, *25*, 2459–2468.
41. Huang, S.J.; Hu, Z.W.; Zhong, Y.J.; Huang, K.K.; Li, X.N. Saddle dolomite in Permian-Triassic carbonate rocks and sandstones of Sichuan Basin: Petrology, formation temperature and palaeofluids. *J. Chengdu Univ. Technol.* **2015**, *42*, 129–148.
42. Huang, S.J.; Pan, X.Q.; Lu, J.; Qi, S.C.; Huang, K.K.; Lan, Y.F.; Wang, C.M. Hydrothermal dolomitization and subsequent retrograde dissolution in Qixia Formation, West Sichuan: A case study of incomplete and halfway-back dolomitization. *J. Chengdu Univ. Technol.* **2013**, *40*, 288–300.
43. Jiang, Y.Q.; Tao, Y.Z.; Yifan, G.U.; Wang, J.B.; Qiang, Z.T.; Jiang, N.; Lin, G.; Jiang, C. Hydrothermal dolomitization in Sinian Dengying Formation, Gaoshiti-Moxi area, Sichuan Basin, SW China. *Pet. Explor. Dev.* **2016**, *43*, 54–64. [CrossRef]
44. Xuan, C. Characteristics and exploration strategy of the Middle Permian hydrothermal dolomite in southwestern Sichuan Basin. *Acta Pet. Sin.* **2013**, *34*, 460–466.
45. Meng, W.B.; Wu, H.Z.; Li, G.R.; Zhang, X.Q.; Lü, Z.X. Dolomitization mechanisms and influence on reservoir development in the Upper Permian Changxing Formation in Yuanba area, northern Sichuan Basin. *Acta Pet. Sin.* **2014**, *30*, 699–708.

46. Liu, S.G.; Huang, W.M.; Jansa, L.F.; Wang, G.Z.; Song, G.Y.; Zhang, C.J.; Wei, S.; Wenxin, M.A. Hydrothermal dolomite in the Upper Sinian (Upper Proterozoic) Dengying formation, East Sichuan Basin, China. *Acta Geol. Sin.* **2014**, *88*, 1466–1487. [CrossRef]
47. Cui, W.D. The sedimentation, Diagenesis and influence upon Reservoir of Feixianguan Formation in Lower Triassic Series, Northwest Sichuan. Master's Thesis, Southwest Petroleum University, Chengdu, China, 2003; p. 141.
48. Rong, H.; Jiao, Y.Q.; Wu, L.Q.; Gu, Y.; Zhang, L.Y. Relationship between heterogeneity and seismic velocities of the Yudongzi Triassic oolitic reservoirs in the Erlangmiao area, northwest Sichuan Basin, China. *J. Pet. Sci. Eng.* **2012**, *100*, 81–98. [CrossRef]
49. Rong, H.; Jiao, Y.Q.; Wu, L.Q.; Gu, Y.; Zhang, L.Y.; Li, R.; Zeng, F.P. Effects of diagenesis on the acoustic velocity of the Triassic oolitic shoals in the Yudongzi outcrop of Erlangmiao area, Northwest Sichuan Basin. *J. Earth Sci.* **2012**, *23*, 542–558. [CrossRef]
50. Hao, Y.; Zhou, J.G.; Zhang, J.Y.; Ni, C.; Gu, M.F. Characteristics and controlling factors of dolomite reservoir in Yudongliang Area, Sichuan Basin. *J. Southwest Pet. Univ. (Sci. Technol. Ed.)* **2011**, *33*, 25–30.
51. Rong, H.; Jiao, Y.Q.; Wu, L.Q.; Li, R.; Wang, R.; Lu, C. Oolitic shoal composition and its implication of Feixianguan formation in Yudongzi section of Erlangmiao, Jiangyou, Sichuan, China. *Earth Sci.* **2010**, *35*, 125–136.
52. Liu, J.H.; Y, Z.X.; Wang, S.L.; Wei, J.S. Geologic-tectonic evolutional characteristics and prospecting potential for ISL-amenable sandstone-type uranium deposits in Sichuan basin. *Uranium Geol.* **2005**, *21*, 321–330.
53. Xu, S.Q.; Hong, H.T.; Zhang, G.R.; He, Z.H.; Hu, H.Z.; Chen, S. Main controlling factor analysis on oolitic reservoir development of lower Triassic Feixianguan Formation in Sichuan Basin. *Nat. Gas Explor. Dev.* **2004**, *27*, 1–3.
54. Chen, H.D.; Zhong, Y.J.; Hou, M.C.; Lin, L.B.; Dong, G.Y.; Liu, J.H. Sequence styles and hydrocarbon accumulation effects of carbonate rock platform in the Changxing-Feixianguan formations in the northeastern Sichuan Basin. *Oil Gas Geol.* **2009**, *30*, 539–547.
55. Yang, Y.Y.; Li, G.R.; Deng, Y. Reservoir characteristics of the Feixianguan Formation in Kaijiang-Liangping continental shelf flanks, northeastern Sichuan Basin. *Oil Gas Geol.* **2012**, *33*, 736–742.
56. Zhang, Z.X.; Wang, Q.Z.; Wang, N.J.; Li-Zhong, H.U.; Yang, X. Relationship Between Order Degree of Dolomite and Parasequence—Majiagou Formation of Ordovician in Ordos Basin. *J. Chengde Pet. Coll.* **2012**, *14*, 13–17.
57. Huang, S.J. The degree of order and forming conditions of the dolomite of the third and fourth members of lower triassic Jialingjiang Formation in Longmenxia, Quxian, Sichuan. *J. Mineral. Petrol.* **1985**, *5*, 57–62.
58. Zhong, Q.Q.; Huang, S.J.; Zou, M.L.; Tong, H.P.; Huang, K.K.; Zhang, X.H. Controlling factors of order degree of dolomite in carbonate rocks: A case study from Lower Paleozoic in Tahe Oilfield and Triassic in northeastern Sichuan Basin. *Lithol. Reserv.* **2009**, *21*, 50–55.
59. Ni, X.; Chen, H.; Tian, J.; Wei, D. Sedimentary framework of Changxing-Feixianguan Formations and its control on reservoiring in northeastern Sichuan basin. *Oil Gas Geol.* **2007**, *28*, 458–465.
60. Wei, G.Q. Sedimentary system of platformal trough of Feixianguan Formation of Lower Triassic in Northern Sichuan Basin and its evolution. *Acta Sediment. Sin.* **2004**, *13*, 573–574.
61. Pierson, B.J. The control of cathodoluminescence in dolomite by iron and manganese. *Sedimentology* **2010**, *28*, 601–610. [CrossRef]
62. Huang, S.J.; Huang, K.K.; Jie, L.; Lan, Y.F. The relationship between dolomite textures and their formation temperature: A case study from the Permian-Triassic of the Sichuan Basin and the Lower Paleozoic of the Tarim Basin. *Pet. Sci.* **2014**, *11*, 39–51. [CrossRef]
63. Ali, A.E.; Barbin, V.; Calas, G.; Cervelle, B.; Ramseyer, K.; Bouroulec, J. Mn^{2+}-activated luminescence in dolomite, calcite and magnesite: quantitative determination of manganese and site distribution by EPR and CL spectroscopy. *Chem. Geol.* **1993**, *104*, 189–202. [CrossRef]
64. Hardie, L.A. Dolomitization: A critical view of some current views. *J. Sediment. Res.* **1987**, *57*, 166–183. [CrossRef]
65. Katz, A. Zoned dolomite crystals. *J. Geol.* **1971**, *79*, 38–51. [CrossRef]
66. Frank, T.D.; Lohmann, K.C. Diagenesis of fibrous magnesian calcite marine cement: Implications for the interpretation of δ 18 O and δ 13 C values of ancient equivalents. *Geochim. Cosmochim. Acta* **1996**, *60*, 2427–2436. [CrossRef]

67. Charef, A.; Sheppard, S.M.F. Carbon and oxygen isotope analysis of calcite or dolomite associated with organic matter. *Chem. Geol.* **1984**, *46*, 325–333. [CrossRef]
68. Allan, J.R.; Wiggins, W.D. Dolomite reservoirs—Geochemical techniques for evaluating origin and distribution (AAPG Continuing Education Course Note Series No. 36). *Tulsa: AAPG* **1993**, *36*, 26–129.
69. Keith, M.L.; Weber, J.N. Carbon and oxygen isotopic composition of selected limestones and fossils. *Geochim. Cosmochim. Acta* **1964**, *28*, 1787–1816. [CrossRef]
70. Chen, D.; Gong, E.; Liang, J.; Chen, X.H. The carbon and oxygen stable isotopic compositions and sedimentary environment of the lacustrine carbonate from the Upper Cretaceous Yixian Formation, Western Liaoning, NE China. *Acta Geol. Sin.* **2011**, *85*, 987–992.
71. Mcarthur, J.M.; Howarth, R.J.; Bailey, T.R. Strontium isotope stratigraphy: LOWESS Version 3: Best fit to the marine Sr-isotope curve for 0–509 Ma and accompanying look up table for deriving numerical age. *J. Geol.* **2001**, *109*, 155–170. [CrossRef]
72. Baker, P.A.; Burns, S.J. Occurrence and formation of dolomite in organic-rich continental margin sediments. *Am. Assoc. Pet. Geol. Bull.* **1985**, *69*, 1917–1930.
73. Green, D.G. Fault and conduit controlled burial dolomitization of the Devonian west-central Alberta Deep Basin. *Bull. Can. Pet. Geol.* **2005**, *53*, 101–129. [CrossRef]
74. Richter, F.M.; Liang, Y. The rate and consequences of Sr diagenesis in deep-sea carbonates. *Earth Planet. Sci. Lett.* **1993**, *117*, 553–565. [CrossRef]
75. Horita, J. Oxygen and carbon isotope fractionation in the system dolomite-water-CO2 to elevated temperatures. *Geochim. Cosmochim. Acta* **2014**, *129*, 111–124. [CrossRef]
76. Coplen, T.; Kendall, C.; Hopple, J. Comparison of stable isotope reference sample. *Nature* **1983**, *302*, 236–238. [CrossRef]
77. Mu, S.G.; Zhou, M.; Hua, Y.C. Dolomite genetic types in Feixianguan Formation of Lower Triassic Series in Northeast Area of Sichuan. *Nat. Gas Ind.* **1994**, *14*, 23–27.
78. Korte, C.; Kozur, H.W.; Veizer, J. δ 13 C and δ 18 O values of Triassic brachiopods and carbonate rocks as proxies for coeval seawater and palaeotemperature. *Palaeogeogr. Palaeoclimatol. Palaeoecol.* **2005**, *226*, 287–306. [CrossRef]
79. Ren, J.G.; Huang, Y.P.; Fang, Z.S. Oxygen and hydrogen isotope composition of meteoric water in the tropical West Pacific Ocean. *Acta Oceanol. Sin.* **2000**, *22*, 60–64.
80. Yuan, X.P.; Liu, J.B. Research history and progress on reflux seepage dolostone. *J. Palaeogeogr.* **2012**, *14*, 219–228.
81. Consonni, A.; Ronchi, P.; Geloni, C.; Battistelli, A.; Grigo, D.; Biagi, S.; Gherardi, F.; Gianelli, G. Application of numerical modelling to a case of compaction-driven dolomitization: A Jurassic palaeohigh in the Po Plain, Italy. *Sedimentology* **2010**, *57*, 209–231. [CrossRef]